Alexandria Engineering Journal (2022) 61, 7303–7313

Alexandria University

Alexandria Engineering Journal

www.elsevier.com/locate/aej
www.sciencedirect.com

Analytical and numerical studies for wave generated by submarine landslide

Ikha Magdalena *, **Kemal Firdaus, Devina Jayadi**

Faculty of Mathematics and Natural Sciences, Bandung Institute of Technology, Jl. Ganesha No. 10, Bandung, West Java 40132, Indonesia

Received 6 August 2021; revised 15 December 2021; accepted 28 December 2021
Available online 22 January 2022

KEYWORDS

Submarine landslides;
Non-linear shallow water equations;
Staggered finite volume;
Analytical solution;
Generated tsunami waves

Abstract In this research, we investigate how submarine landslides are able to produce extremely damaging tsunami waves and estimate the maximum height of the waves in question using a mathematical model. The model is based on the non-linear shallow water equations, which are solved numerically using the finite volume method on a staggered grid. We also derive a new analytical solution in order to obtain a description of surface waves generated by a submarine landslide. To validate the numerical model, several benchmark tests are conducted by comparing the results from the numerical scheme to those obtained from the analytical solution, experimental data, or other numerical results. After validation, the scheme is implemented on the real topography of Palu Bay to simulate the generation of tsunami waves by submarine landslides. The simulations provide excellent results. Accurate estimates of the maximum tsunami wave amplitude are produced by the numerical scheme, confirmed by data from records of the 2018 Palu tsunami.

1. Introduction

On 28 September 2018, a magnitude 7.5 earthquake occurred 70 km north of Palu, Sulawesi, Indonesia (US Geological Survey [1]; Japan Meteorologgical Agency [2]), and was identified as a supershear strike-slip earthquake with a rupture velocity of 4.1 km/s (Bao et al. [3]). A tsunami generated by the earthquake struck the coast, leveling houses, washing away vehicles, and destroying the coastal area. Several studies have shown that landslides caused the destructive tsunami (Takagi et al. [4], Sassa and Takagawa [5], and Arikawa et al. [6]). The dominant tsunami-generating landslide was submarine and occurred near the northwest entrance of the bay (Pakoksung et al. [7]). This phenomenon left the area devastated. Submarine landslides near the bay were identified as the generators of these destructive waves. The ability to predict the heights of similarly-generated tsunami waves would facilitate the conception of appropriate protective structures or regulations, thus reducing the amount of damage caused by the waves.

In 1992, Heinrich [8] studied landslides experimentally. However, conducting physical experiments is a very expensive endeavor. Therefore, recent studies have focused on measuring wave heights generated by submarine landslides through mathematical modeling. In this study, we are interested in analyzing the tsunami wave's features, particularly the wave form, and

* Corresponding author.
E-mail address: ikha.magdalena@math.itb.ac.id (I. Magdalena).
Peer review under responsibility of Faculty of Engineering, Alexandria University.

https://doi.org/10.1016/j.aej.2021.12.069

the different types of tsunami-causing submarine landslides. Many researchers have presented numerical procedures to approximate different models in order to study tsunamis. One such model is the Boussinesq-type Equation, which has become a popular mathematical model for tsunami generation simulations. Several examples of researchers who have studied tsunamis using Boussinesq-type models are Gobbi and Kirby [9], who implemented the model to demonstrate the non-linearity of the waves, and Fuhrman and Madsen [10], who developed a high order Boussinesq approximation and a numerical scheme based on the highly-accurate Boussinesq-type formulation, which was then used to simulate several different cases. However, Hervouet and Jankowski [11] stated that models based on the Boussinesq equations are not computationally advantageous due to the approximations' high order. Other models have also been proposed. Kozelkov et al. [12] implemented a numerical solution to approximate the Navier-Stokes Equations for the study of multi-phase flows, while Lynett and Liu [13] simulated submarine landslides using the Boundary Integral Equation Model (BIEM). Studies of wave phenomena that approach the subject analytically and numerically include [14,15]'s use of the nonlinear Schrodinger equation, [16]'s approximate solutions for KdV equations using a Caputo-Fabrizo fractional derivative, [17]'s generalized ρ-Laplace transform method and heat balanced integral method, [18]'s implementation of a novel numerical method for solving differential equations with fractional variable-order, [19]'s computational solutions of fuzzy Volterra integral equations with degenerate kernels, [20]'s analysis of El Nino-Southern Oscillation with the aid of an Adams-Bashforth numerical scheme, [21]'s extension of the optimal auxiliary function method to general partial differential equations, and [22]'s solutions of the fractional differential equations where the second members are constant functions, polynomial functions, exponential functions, trigonometric functions, or Mittag-Leffler functions. Such models still involve additional complexity and high computational cost.

Therefore, in this study, we investigate the tsunami wave forms over several different bottom profiles using the non-linear shallow water equations. This model is chosen because we have confirmed that it is efficient, relatively simple, and robust, as written in Andadari and Magdalena [23], Magdalena et al. [24,25], Magdalena and Rif'atin [26] for the linear case, and Pudjaprasetya and Magdalena [27], Magdalena [28], Magdalena et al. [29] for the non-linear case. Here, a finite volume method on a staggered grid with a simple approximation for the advection term is constructed in order to solve the model numerically. We also derived an analytical solution for surface waves generated by a landslide over a flat bottom. The numerical scheme is then used to simulate results from several previous studies. Simulation results for the flat bottom case are validated using the analytical solution. Experimental data from previous studies are used to validate simulations of tsunamis generated over bottom profiles of non-constant depth. After conducting benchmark tests, we apply the numerical scheme to the topography of Palu Bay in order to illustrate the range of possible tsunami heights during the observation period.

The rest of the paper is structured as follows. The derivation of the analytical solution is presented in Section 2. An explanation of the shallow water equations are provided in Section 3. The corresponding computational staggered finite volume scheme is described in Section 4. We then compare the results of the numerical and the experimental data in Section 5 and present our conclusions in Section 6.

2. Analytical solution

In this section, we derive the analytical solution for surface waves generated by a landslide over a flat bottom, as illustrated in Fig. 1.

Consider a landslide with the characteristic length L and the characteristic height H. It moves with velocity V over a constant depth d. We use $\eta(x,t)$ and $B(x,t)$ to denote the dimensional surface elevation and bottom movement functions, respectively. These variables are then normalised by $x = x\prime/L, z = z\prime/d, t = t\prime\sqrt{gd}/L, \eta(x,t) = \eta\prime(x\prime,t\prime)/H, B(x,t) = B\prime(x\prime,t\prime)/H$, resulting in the following dimensionless governing equations:

$$\mu^2\phi_{xx} + \phi_{zz} = 0, -1 < z < 0, \tag{1}$$

$$\phi_z = \mu^2 B_t, z = -1, \tag{2}$$

$$\phi_z = \mu^2\eta_t, z = 0, \tag{3}$$

$$\phi_t + \eta = 0, z = 0. \tag{4}$$

Here, $\phi(x,z,t) = \phi\prime(x,z,t)/(\epsilon L\sqrt{gd})$ is the normalised velocity potential and $\mu = d/L$ controls the frequency dispersion. Differentiating Eq. (4) with respect to x and then substituting η_t from Eq. (3) yields

$$\phi_z + \mu^2\phi_{tt} = 0. \tag{5}$$

To solve the governing equations above, we solve the model analytically using Fourier and Laplace transforms. Recall the formula of Fourier and Laplace transforms followed by the inverse:

$$\mathscr{L}(f) = \bar{f}(s) = \int_0^\infty e^{-st} f(t)dt;$$

$$\mathscr{L}^{-1}(\bar{f}) = f(t) = \frac{1}{2\pi i}\int_\tau e^{st}\bar{f}(s)ds,$$

$$\mathscr{F}(f) = \tilde{f}(k) = \int_{-\infty}^\infty e^{-ikx} f(x)dx;$$

$$\mathscr{F}^{-1}(\tilde{f}) = f(x) = \frac{1}{2\pi}\int_{-\infty}^\infty e^{ikx}\tilde{f}(k)dk.$$

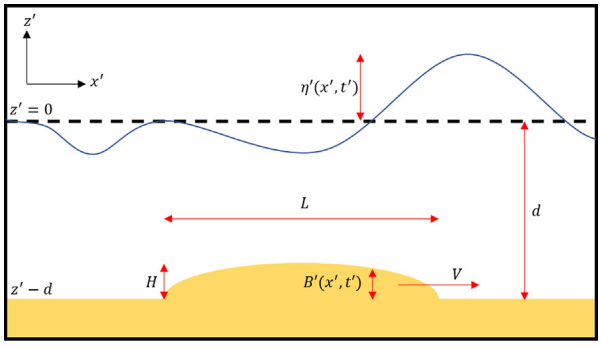

Fig. 1 Illustration of the landslide-generated waves in constant depth.

The notation τ is a vertical line to the right of all singularities of the integrand function in the complex s-plane. The combined Fourier-Laplace transformation can be expressed as

$$\mathscr{L}(\mathscr{F}(f(x,t))) = \tilde{\tilde{f}}(k,s) = \int_{-\infty}^{\infty} e^{-ikx} \int_{0}^{\infty} e^{-st} f(x,t)\,dt\,dx.$$

An effective application of Laplace-Fourier transforms have also been used by Avcı et al. [30]. Applying Laplace-Fourier transform to the governing Eqs. 1, 2, 4, Eq. (5), we obtain

$$\tilde{\tilde{\phi}}_{zz} - k^2\mu^2\tilde{\tilde{\phi}} = 0, \tag{6}$$

$$\tilde{\tilde{\phi}}_{z}(k,-1,s) = \mu^2 s(\tilde{\tilde{B}}(k,s) - \frac{1}{s}\tilde{B}(k,0)), \tag{7}$$

$$s\tilde{\tilde{\phi}}(k,0,s) + \tilde{\tilde{\eta}}(k,s) = 0, \tag{8}$$

$$\phi_{z}(k,0,s) = -s^2\mu^2\tilde{\tilde{\phi}}(k,0,s). \tag{9}$$

Solving Eq. (6) using the method of characteristics yields

$$\tilde{\tilde{\phi}}(k,z,s) = P(k,s)\cosh(\mu k z) + Q(k,s)\sinh(\mu k z). \tag{10}$$

Substituting Eq. (10) when $z = 0$ into the boundary condition in Eq. (9) gives us

$$Q(k,s) = -\frac{s^2\mu}{k}P(k,s) \tag{11}$$

and

$$\tilde{\tilde{\phi}}(k,z,s) = P(k,s)\cosh(\mu k z) - \frac{s^2\mu}{k}P(k,s)\sinh(\mu k z). \tag{12}$$

By differentiating Eq. (12) with respect to z and applying the boundary condition Eq. (7), we obtain

$$P(k,s) = \frac{\mu s}{\cosh(\mu k)}\frac{\tilde{\tilde{B}}(k,s) - \frac{1}{s}\tilde{B}(k,0)}{-k\tanh(\mu k) - s^2\mu} = \frac{\mu s}{\cosh(\mu k)}\frac{\frac{1}{s}\tilde{B}(k,0) - \tilde{\tilde{B}}(k,s)}{k\tanh(\mu k) + s^2\mu},$$

$$Q(k,s) = -\frac{s^2\mu}{k}\frac{\mu s}{\cosh(\mu k)}\frac{\tilde{\tilde{B}}(k,s) - \frac{1}{s}\tilde{B}(k,0)}{-k\tanh(\mu k) - s^2\mu} - \frac{\mu^2 s^3}{k\cosh(\mu k)} \times \frac{\tilde{\tilde{B}}(k,s) - \frac{1}{s}\tilde{B}(k,0)}{-k\tanh(\mu k) - s^2\mu}.$$

Eq. (12) is evaluated at $z = 0$ and substituted into Eq. (8) by involving the new definition for $P(k,s)$. We then get the analytical solution for wave elevation generated by a landslide:

$$\tilde{\tilde{\eta}}(k,s) = \frac{\mu}{\cosh(\mu k)}\frac{s^2\tilde{\tilde{B}}(k,s) - s\tilde{B}(k,0)}{\mu s^2 + k\tanh(\mu k)}. \tag{13}$$

In this case, we will show a particular example. Assume we take normalized Gaussian-shaped landslide to be simulated analytically, written as

$$B(x,t) = e^{-8(x-Frt)^2}.$$

This shape was chosen because its form is similar to the shape of a simple mound. Hence, its Fourier and Laplace-Fourier transforms are

$$\tilde{B}(k,t) = \frac{\sqrt{8\pi}}{8}e^{-\frac{1}{32}k^2 - ikFrt},$$

$$\tilde{\tilde{B}}(k,s) = \frac{\sqrt{2\pi}}{4}\frac{e^{-\frac{1}{32}k^2}}{s + ikFr},$$

respectively. Substitution of the transformed function B into Eq. (13) yields an altered version of the transformed surface elevation,

$$\tilde{\tilde{\eta}} = \frac{e^{-\frac{1}{32}k^2}\sqrt{2\pi}}{4\cosh(\mu k)}\frac{-s\alpha}{(s^2+\beta^2)(s+\alpha)},$$

with $\alpha = ikFr$ and $\beta = \sqrt{\frac{k}{\mu}\tanh(\mu k)}$. To obtain the surface elevation, we take the inverse of $\tilde{\tilde{\eta}}$ thus

$$\eta = \frac{1}{2\pi}\int_{-\infty}^{\infty} e^{ikx}\left(\frac{1}{2\pi i}\int_{\tau} e^{st}\tilde{\tilde{\eta}}\,ds\right)dk$$

$$= \frac{1}{2\pi}\int_{-\infty}^{\infty} e^{ikx}\left(\frac{1}{2\pi i}\int_{\tau} e^{st}\frac{e^{-\frac{1}{32}k^2}\sqrt{2\pi}}{4\cosh(\mu k)}\frac{-s\alpha}{(s^2+\beta^2)(s+\alpha)}\,ds\right)dk$$

$$= -\frac{\sqrt{2\pi}}{16\pi^2 i}\int_{-\infty}^{\infty}\frac{e^{ikx}e^{-\frac{1}{32}k^2}}{\cosh(\mu k)}\left(\int_{\tau} e^{st}\frac{s\alpha}{(s^2+\beta^2)(s+\alpha)}ds\right)dk. \tag{14}$$

Note that the analytical solution for landslide-generated waves as written in Eq. (14) is an implicit function. Therefore, we will solve the integrand using by residual integration. First, consider $f(s) = \frac{s\alpha}{(s^2+\beta^2)(s+\alpha)}$ as a function with three poles: $s = -\alpha,\ i\beta,\ -i\beta$. Then, the inner integral will be calculated in the complex domain where τ is a vertical line to the line of all singularities of integrand function in the complex s-plane. By the Cauchy theorem, we obtain

$$\int_{\tau} e^{st}f(s)\,ds = \left\{2\pi i\left[{}^{Res}_{s=\alpha}e^{st}f(s) + {}^{Res}_{s=i\beta}e^{st}f(s) + {}^{Res}_{s=-i\beta}e^{st}f(s)\right], 0.\right.$$

For $t > 0$,

$$\int_{\tau} e^{st}f(s)\,ds = 2\pi i\left[-\frac{\alpha^2}{e^{t\alpha}\alpha^2 + e^{t\alpha}\beta^2} + \frac{ie^{it\beta}\alpha\beta}{-2\beta^2 + 2i\beta\alpha} + \frac{ie^{-it\beta}\alpha\beta}{2\beta^2 + 2i\beta\alpha}\right]$$

$$= 2\pi i\left[\frac{\alpha^2\cos(\beta t) + \alpha\beta\cos(\beta t) - \alpha^2 e^{-\alpha t}}{\alpha^2+\beta^2}\right].$$

Then, η can be explicitly expressed as

$$\eta(x,t) = -\frac{\sqrt{2\pi}}{16\pi^2 i}\int_{-\infty}^{\infty} \times \frac{e^{ikx}e^{-\frac{1}{32}k^2}}{\cosh(\mu k)}2\pi i\left[\frac{\alpha^2\cos(\beta t) + \alpha\beta\cos(\beta t) - \alpha^2 e^{-\alpha t}}{\alpha^2+\beta^2}\right]dk$$

$$= -\frac{\sqrt{2\pi}}{8\pi}\int_{-\infty}^{\infty}\frac{e^{ikx}e^{-\frac{1}{32}k^2}}{\cosh(\mu k)}\left[\frac{\alpha^2\cos(\beta t) + \alpha\beta\cos(\beta t) - \alpha^2 e^{-\alpha t}}{\alpha^2+\beta^2}\right]dk.$$

Notice that the integrand is an even function, so that

$$\eta(x,t) = \frac{\sqrt{2\pi}}{4\pi}\int_{0}^{\infty}\frac{e^{ikx}e^{-\frac{1}{32}k^2}}{\cosh(\mu k)} \times \left[\frac{\alpha^2 e^{-\alpha t} - \alpha^2\cos(\beta t) - \alpha\beta\cos(\beta t)}{\alpha^2+\beta^2}\right]dk. \tag{15}$$

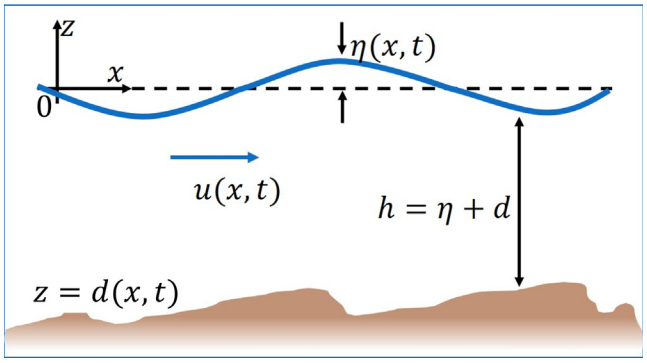

Fig. 2 Illustration of Non-linear Shallow Water Equations model.

Finally, we will solve the integral using numerical integration to approximate the analytical result as shown in SubSection 5.4.

3. Mathematical model

This section will explain the mathematical model that we use to investigate tsunami-causing landslides. The model that we apply here is based on the non-linear shallow water equations (NSWE). The model assumes that fluid flow is incompressible with uniform fluid density, the vertical component of the fluid particles is neglected, and the horizontal velocity is assumed to be the same for all depths. The NSWEs are derived by averaging the Navier-Stokes equations over vertical coordinates [31] and consist of two hyperbolic equations, the mass conservation (16) and momentum balance (17) equations, written as

$$h_t + (hu)_x = 0, \tag{16}$$

$$u_t + uu_x + g\eta_x = 0. \tag{17}$$

Here, $\eta(x,t)$ denotes the free surface elevation that is measured from the undisturbed water level $z = 0, h(x,t) = \eta(x,t) + d(x,t)$ represents the water thickness, and $u(x,t)$ is the horizontal velocity, as described in Fig. 2. In this scenario, the bottom topography d is a function of x and t since the bottom moves as time progresses.

4. Numerical method

Here, we solve the model numerically using the finite volume method on a staggered grid. This method has two major advantages: First, it enforces conservation of quantities when discretizing them. Second, the schemes takes full advantage of arbitrary meshes to approximate complex geometries [32]. The success of this method in solving partial differential equations can be found in [33,34]. Suppose the length of our observation domain is $[0, L]$. The domain is then partitioned in a staggered manner into half and full grids with a spatial step Δx, as illustrated in Fig. 3.

Eq. (16) will be calculated in cells $[x_{j-\frac{1}{2}}, x_{j+\frac{1}{2}}]$, or cells marked by blue lines, while Eq. (17) will be calculated in cells $[x_j, x_{j+1}]$, or cells marked by red lines. On the staggered grid, wave elevation $\eta(x,t)$ and depth $h(x,t)$ are only calculated at full grid points x_j, while $u(x,t)$ is only calculated at half-grid points $x_{j+\frac{1}{2}}$. Using the finite volume method, the numerical approximation of Eq. (16) and Eq. (17) is written below.

$$\frac{h_j^{n+1} - h_j^n}{\Delta t} + \frac{({}^*hu)_{j+\frac{1}{2}}^n - ({}^*hu)_{j-\frac{1}{2}}^n}{\Delta x} = 0, \tag{18}$$

$$\frac{u_{j+\frac{1}{2}}^{n+1} - u_{j+\frac{1}{2}}^n}{\Delta t} + g\frac{\eta_{j+1}^{n+1} - \eta_j^{n+1}}{\Delta x} + (uu_x)_{j+\frac{1}{2}}^n = 0, \tag{19}$$

where subscripts and superscripts denote the spatial and temporal grid indices, respectively. Note that though values of h are required to calculate hu, h does not have a value on half-grid points. Therefore, in this scheme, we approximate h using the notation ${}^*h$, which will be determined using the first-order upwind scheme which depends on the flow velocity. The upwind scheme is described as follows:

$${}^*h_{j+\frac{1}{2}}^n = \begin{cases} h_j^n, & \text{if } u_{j+\frac{1}{2}}^n > 0, \\ h_{j+1}^n, & \text{if } u_{j+\frac{1}{2}}^n < 0. \end{cases} \tag{20}$$

One of the challenges in solving the NSWEs numerically is finding an appropriate approximation for the advection term, which is denoted by uu_x. Here, we propose a simple method to approximate uu_x by defining the term as

$$uu_x = \frac{qu_x}{h} = \frac{q}{h}\frac{\partial u}{\partial x}, \tag{21}$$

with $q = hu$. Then, Eq. (21) can be written as

$$(uu_x)_{j+\frac{1}{2}} = \frac{\bar{q}_{j+\frac{1}{2}}}{\bar{h}_{j+\frac{1}{2}}}\left(\frac{{}^*u_{j+1} - {}^*u_j}{\Delta x}\right), \tag{22}$$

where

$$\bar{h}_{j+\frac{1}{2}} = \frac{1}{2}(h_j + h_{j+1}), \tag{23}$$

$$\bar{q}_j = \frac{1}{2}(q_{j+\frac{1}{2}} + q_{j-\frac{1}{2}}), \tag{24}$$

$$q_{j+\frac{1}{2}} = {}^*h_{j+\frac{1}{2}}u_{j+\frac{1}{2}}. \tag{25}$$

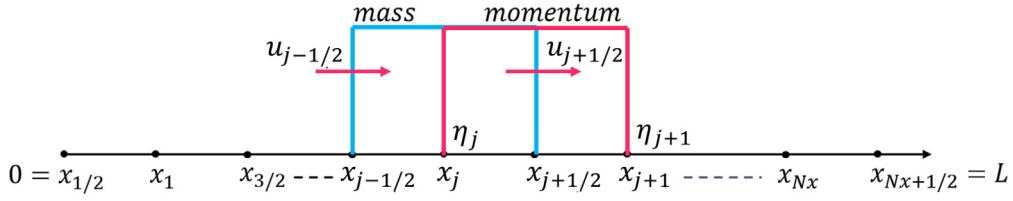

Fig. 3 Staggered grid illustration.

The value of ${}^{*}u_j$ is approximated using a first-order upwind scheme.

$$ {}^{*}u_j = \begin{cases} u_{j-\frac{1}{2}}, & \text{if } \bar{q}_j \geqslant 0, \\ u_{j+\frac{1}{2}}, & \text{if } \bar{q}_j < 0. \end{cases} \tag{26} $$

In order to simulate the propagation of waves over a dry bed where $h \leqslant 0$, it is necessary for the numerical scheme to adapt to the moving wet-dry interface. Therefore, we compute the discrete formula for Eq. (19) only if the water depth is greater than a minimum threshold depth $h = 0$. This step is called the wet-dry procedure. Additionally, the selection of Δx and Δt follows the Von Neumann stability condition, $0 \leqslant \sqrt{d_0}\frac{\Delta t}{\Delta x} \leq 1$, with d_0 as the flat bottom depth. [29]35.

5. Result and discussion

Here, we will implement the numerical scheme that we have formulated above to simulate and study the Palu tsunami's elevation. Before that, we will validate our scheme using several previous models and cases. First, we compare our numerical results to experimental data from Synolakis [36] in order to observe the ability of our scheme to reproduce the wave run-up over a dry sloping bottom. The second test aims to confirm the capability of our computational scheme to simulate the analytical wave generated by movement of seafloor over a constant depth. Third, we simulate landslides using the triangular box and sliding mound set-ups previously used by Heinrich and Lynett, respectively. After validation, we will further investigate the submarine landslide preceding the 2018 Palu Tsunami.

5.1. Run-up over a sloping bottom by Synolakis

Here, the accuracy of our numerical scheme to simulate wave run-up over a sloping bottom will be evaluated by comparing the numerical results with the experimental data in Synolakis [36]. The initial conditions and parameters used in this simulation will be selected according to the set-up of the experiment.

The wave tank in Synolakis' experiment has a length of 31.73 m, a width of 39.97 cm, and a depth of 60.96 cm. The waves first propagate from a position of L_g, which is the edge of a sloping beach with $L_g = \frac{1}{\gamma}\text{arccosh}\sqrt{20}$ and a slope angle of 1/19.85. We use the following initial conditions:

$$ \eta(x,0) = A\text{sech}^2(\gamma(x - x_0)), \tag{27} $$

with

$$ u(x,0) = \eta(x,0)\sqrt{\frac{g}{H}}, \tag{28} $$

The wave amplitude is denoted by A, H is the water depth in the constant domain, g is the acceleration due to gravity, x_0 is the position of the wave crest, and $\gamma = \sqrt{\frac{3A}{4d_0}}$. The initial conditions produce a solitary wave, which propagates towards the sloping beach on the right. The parameters used in this simulation are $g = 1\ m/s^2$ and $d_0 = 1$ m. To avoid the breaking wave phenomenon, we choose $A = 0.0185$ m and $x_0 = 38.34$.

From Fig. 4, we observe that the surface elevations captured from the numerical simulations confirm the experimental data at five different times ($t = 30, 40, 50, 60, 70s$). Thus it is reasonable to claim that our numerical scheme is capable of simulating wave run-up with a moving boundary accurately. In addition, the comparison results also show that the wet-dry procedure in our numerical scheme functions properly in demonstrating the propagation of waves over a dry region, which plays a significant role in achieving the correct results.

5.2. Submarine landslide-generated waves in constant depth

In this case, we will simulate landslide-generated waves as explained in Section 2, which has also been studied by Lo and Liu [37]. A solid landslide, in the shape of a normalized

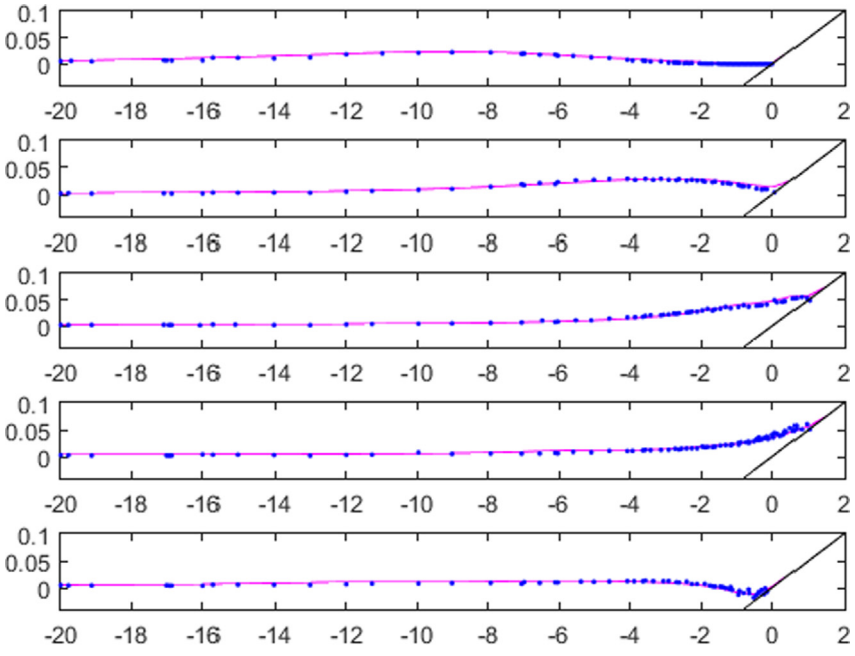

Fig. 4 Wave surfaces at $T = 30, 40, 50, 60, 70$ s.

Table 1 Parameters in the constant depth submarine landslide simulation

Parameter	Value
d	0.4 m
L	2 m
H	0.2 m
V	0.99 m/s

Gaussian curve with the characteristic length L and characteristic height H moving at a constant speed V in constant water depth d, is simulated. The configuration of the sliding mass can be seen in Fig. 1 and the seafloor movement is defined by

$$h(x,t) = -d + He^{-8(x-Frt)^2}. \tag{29}$$

The computation conducted using $\Delta x = 0.01$ and $\Delta t = 0.001$ on a domain $[0, 6]$. The parameters used in this simulation are shown in Table 1. We observed the surface elevation at 4 different times ($t = 0.5, 1.0, 1.5, 2.0$ s). We then compared our numerical result with the analytical solution. This comparison allows us to conclude that our model can accurately simulate the submarine landslide-generated waves in constant depth (see Fig. 5).

5.3. Submarine landslide by Heinrich

Next, we will confirm the capabilities of our numerical scheme to simulate the Heinrich experiment (Heinrich [8]) on the underwater landslide. In Heinrich's experiment, a rigid submarine slide was used to generate waves by allowing a box to freely slide down an inclined plane with an angle of $\theta = 45°$. The experiment was done in a 20 m long, 0.55 m wide, and 1.50 m deep channel in the National Laboratory of Hydraulics of Chatou in France as illustrated in Fig. 6.

The sliding box weighs 140 kg, 0.5 m $\times$ 0.5 m triangular box and has the same width as the flume. The geometrical top of the box was parallel to the still water surface during the experiment. The box, which was equipped with four rollers, slid into the water due to the influence of gravity. It was abruptly stopped at $t = 0.83s$ as it reached the bottom by a 5 cm-high rubber buffer. The shore is modeled by a second plane with a slope of 15°. All surfaces have been carefully checked to match the condition for the numerical simulation as closely as possible, which is friction-less.

The time-variant sliding motion is described by

$$h(x,t) = \begin{cases} 0.268x - 0.268, & \text{if } 0 \leqslant x < 1, \\ x - 1, & \text{if } 1 \leqslant x < x_l, \\ x_l - 1, & \text{if } x_l \leqslant x < x_r, \\ x - 1, & \text{if } x_r \leqslant x < 2, \\ 1, & \text{if } x \geqslant 2, \end{cases} \tag{30}$$

where

$$\begin{aligned} x_l(t) &= x_0 + S(t)\cos\theta - \frac{b}{2}\cos\theta, \\ x_r(t) &= x_0 + S(t)\cos\theta + \frac{b}{2}\cos\theta, \end{aligned} \tag{31}$$

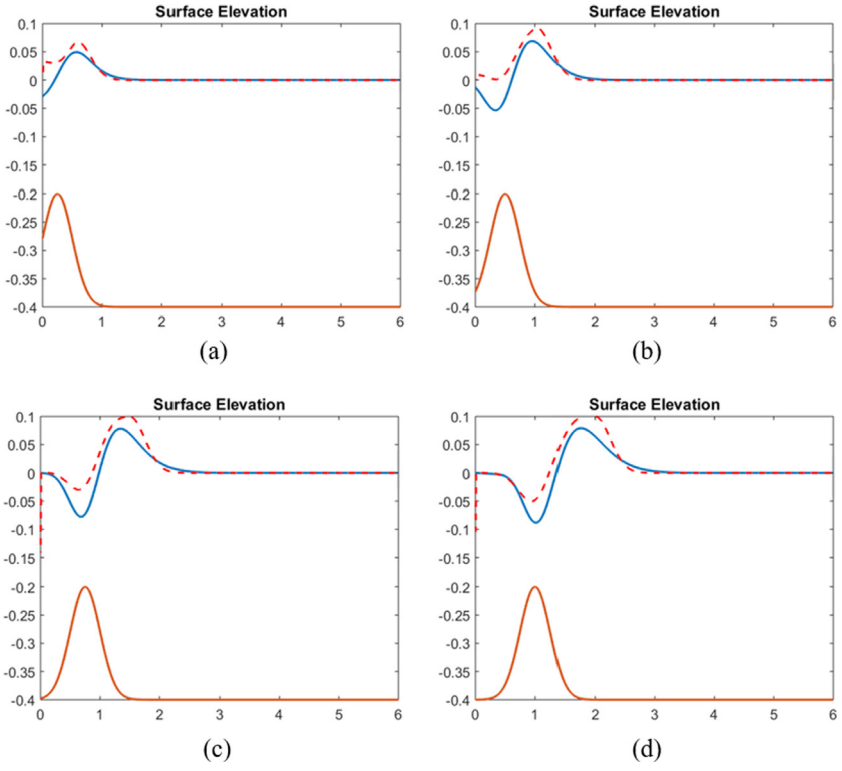

Fig. 5 The comparison of water surface elevation resulted from simulation using NSWEs (blue solid line) and the analytical result (red dash line) at (a) $t = 0.5$ s, (b)$t = 1.0$ s, (c)$t = 1.5$ s, (d)$t = 2.0$ s.

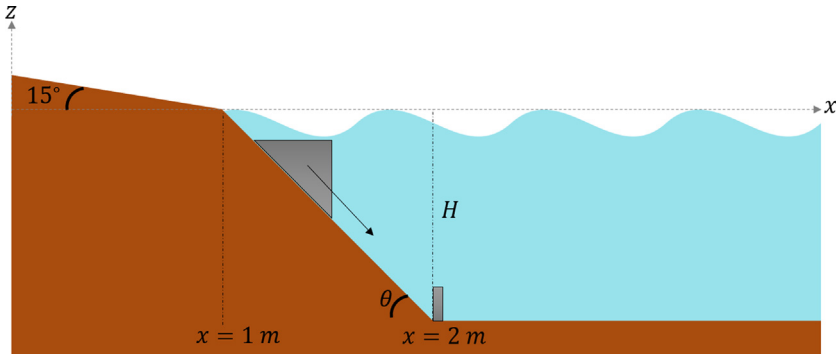

Fig. 6 Experiment set-up illustration of the Heinrich experiment.

Table 2 Parameters in the Heinrich experiment.

Parameter	Value
H	1 m
g	9.812 m/s^2
b	$0.5\sqrt{2}$ m
θ	45°
x_0	1.26 m
S_0	1.4999 m
t_0	0.8058 s

in which x_l and x_r are the left and right ends of the inflection, respectively, while b is the length along the slope between x_l and x_r, θ is the angle of the slope, and x_0 is the initial x position of the sliding box. Here, we define $S(t)$ as

$$S(t) = S_0 \ln\left(\cosh\frac{t}{t_0}\right), \tag{32}$$

corresponds to the resulting motion parallel to the slope, having characteristic length and time scales

$$S_0 = \frac{u_t^2}{a_0}, \quad t_0 = \frac{u_t}{t_0}. \tag{33}$$

The initial landslide acceleration a_0 and terminal landslide velocity u_t are respectively computed by

$$a_0 = g\frac{\gamma - 1}{\gamma - C_m}\sin\theta, \tag{34}$$

$$u_t = \sqrt{gb\frac{\pi(\gamma - 1)}{2C_d}}\sin\theta, \tag{35}$$

where γ is the ratio of the landslide density to the water density, C_m is an appropriate added mass coefficient, and C_d is an appropriate drag coefficient.

The parameters used in this simulation are shown in Table 2. The computation is conducted using $\Delta x = 0.015$ and $\Delta t = 0.001$ on a spatial domain $[0, 4.5]$. We observed the surface elevation at 4 different times ($t = 0.5, 1.0, 1.5, 2.0$ s). Our results are presented in Fig. 7 and compared with the numerical results presented in Kurganov and Petrova [38] who obtained the results using the Non-linear Central-upwind Model. At each observational point, our result is in a good agreement with the corresponding result from [38].

5.4. Submerged landslide by Lynett and Liu

In this case, we use our numerical scheme to simulate the submerged landslide phenomenon originally studied by Lynett and Liu [13] who used a sliding mound to represent a landslide. This sliding mound then generates waves by sliding down an inclined plane with an angle of $\theta = 6°$. The configuration of the sliding mound can be seen in Fig. 8. The time-history of the seafloor is defined by

$$h(x,t) = Sx - \frac{\Delta h}{4}[1 + \tanh(2\cos\theta(x - x_l(t)))][1 - \tanh(2\cos\theta(x - x_r(t)))], \tag{36}$$

where $s = \tan\theta$ is the beach slope, Δh is the maximum vertical height of the slide. To represent the left ends of the inflection, right ends of the inflection, and the resulting motion parallel to the slope, we use the variables $x_l(t), x_r(t)$, and $S(t)$. These are the same as the variables used in Eqs. (31) and (32).

This simulation used the parameters specified in Table 3. The computation is also conducted using $\Delta x = 0.05$ and $\Delta t = 0.005$ on a domain $[0, 7.5]$. We observed the surface elevation at 4 different times ($t = 1.51, 3.00, 4.51, 5.86$ s). Then, we compared our surface elevation results with Lynett and Liu [13]'s dispersive BIEM results. Clearly, our scheme can properly simulate the water surface induced by the downward motion of the sliding mound (see Fig. 9).

5.5. Tsunami generation in Palu

In the previous subsections, we have validated the ability of our numerical scheme to simulate the propagation of tsunami waves generated by underwater landslides. The validations were done by comparing our results against the results from two different models (Heinrich and Lynett). Now, we will identify the maximum height of the tsunami waves near the shore under two scenarios by adapting the triangular box and sliding mound simulations.

5.5.1. Tsunami Palu generated by landslide: triangular box

For this case, we adapt the modeling of hypothetical landslides carried out by Pakoksung et al. [7]. It is suggested that the dominant landslide that caused the tsunami was submarine

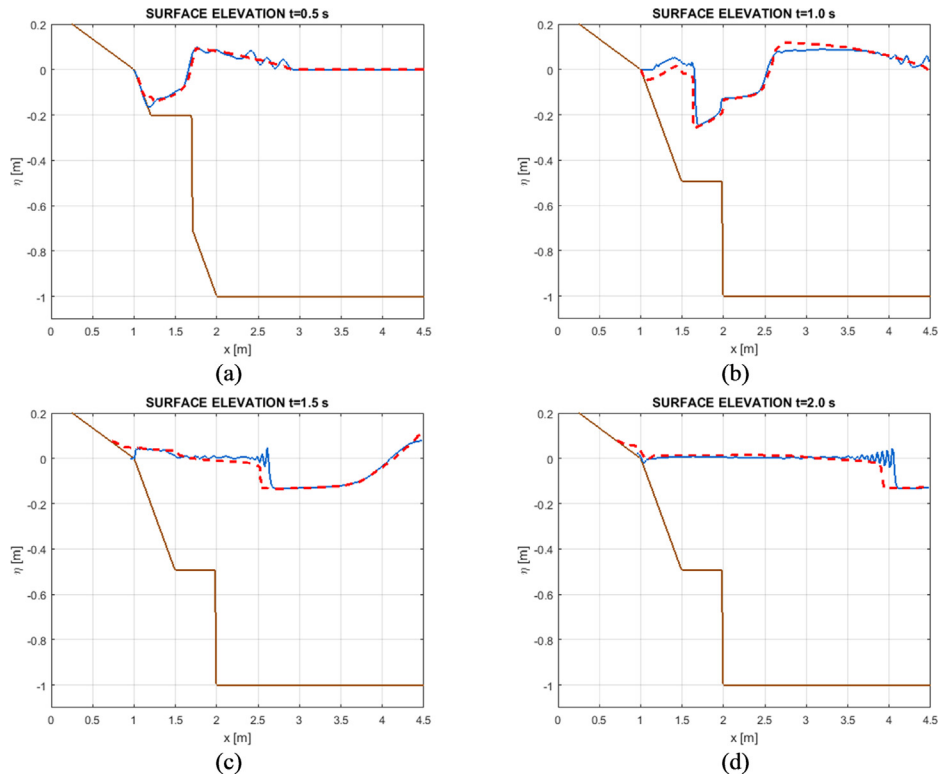

Fig. 7 Water surface elevation η as a result of a submarine landslide using non-linear SWE (blue line) compared with non-linear central-upwind model (red dash-line) at (a) $t = 0.5$ s, (b) $t = 1.0$ s, (c) $t = 1.5$ s, and (d) $t = 2.0$ s.

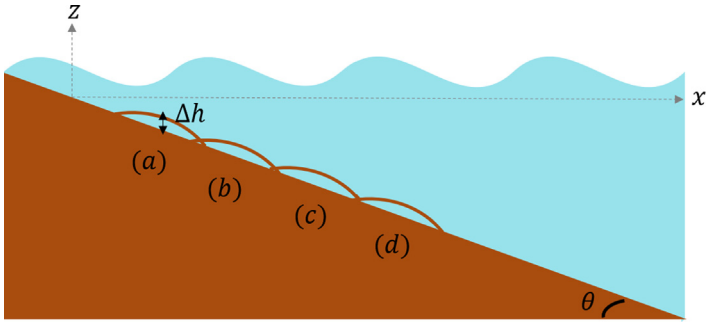

Fig. 8 Illustration of the initial bottom topography for the submerged landslide of Lynett and Liu at (a) $t = 1.51$ s, (b) $t = 3.00$ s, (c) $t = 4.51$ s, and (d) $t = 5.86$ s.

and generated near the entrance of the bay to the northwest. Therefore, calculations were performed at the southern part of Palu Bay around the latitude of $-0.87°$, 20 kilometers away from the shore of Talise Beach. A one-dimensional domain is considered. It is assumed that the submarine landslide occurred at the mouth of the Bay around $-0.63°$ S and 119.76° E and the mass takes 60 s to fall. The data of the landslide location was taken from coastal survey which was conducted by Widiyanto, W. et al. (2019).

Using the concept of a submarine landslide similar to one simulated in SubSection 5.3, we calculate the wave amplitude towards the tsunami propagation time. The simulation is performed using $\Delta x = 0.1$ and $\Delta t = 0.01$. The result of the amplitude of the wave generated by the triangular box submarine landslide is presented in Fig. 10. It is shown that along the time of observation, the maximum amplitude is around 2.7 meters which occurs at about $t = 9$ s. This result has a good agree-

Table 3 Parameters in the Lynett and Liu simulation

Parameter	Value
b	1 m
Δh	0.05 m
θ	6°
x_0	2.379 m
S_0	4.712 m
t_0	3.713 s

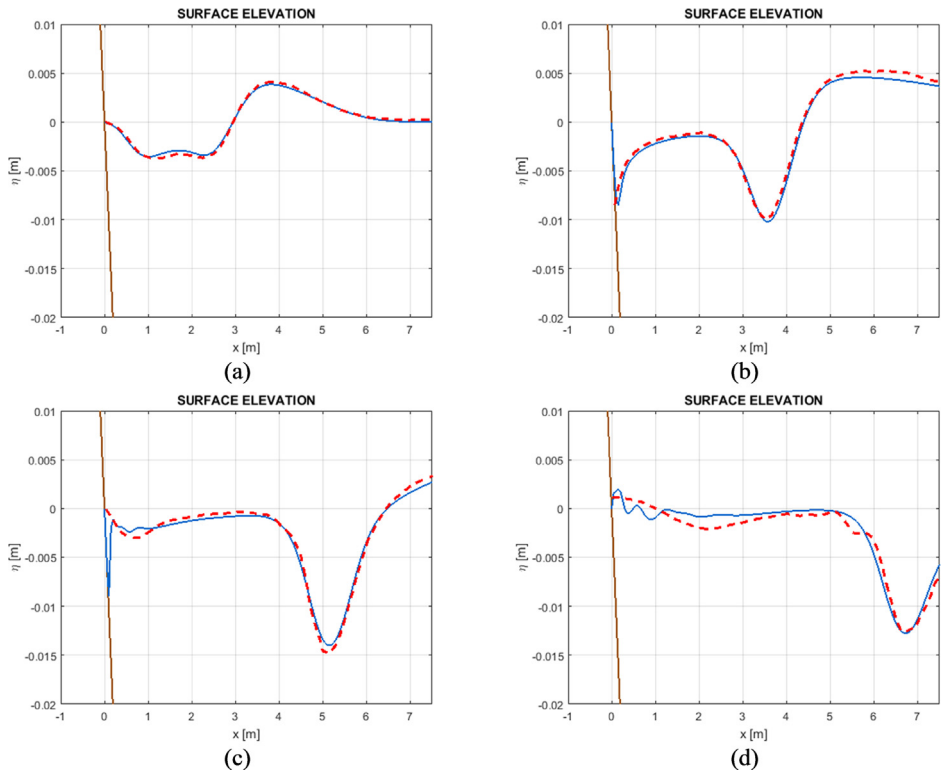

Fig. 9 The comparison of water surface elevation resulted from simulations using NSWE (blue solid line) and the dispersive BIEM by Lynett and Liu (red dash line) at (a) $t = 1.51$ s, (b) $t = 3.00$ s, (c) $t = 4.51$ s, and (d) $t = 5.86$ s.

ment with the maximum tsunami height of the post event field survey at Talise Beach (Widiyanto, W. et al. 2019). However, it can be seen in Fig. 10 that after the waves undergo their maximum amplitude, the amplitude is significantly reduced and remains at a lower value of less than 0.5 meters for the rest of the observation time.

5.5.2. Tsunami Palu generated by landslide: sliding mound

Here, we model a submarine landslide in Palu Bay using the sliding mound approach. We use the same parameters for the spatial partition length and time step, which are $\Delta x = 0.1$ and $\Delta t = 0.01$. The mound takes 60 s to fall. The landslide is assumed to occur at around $-0.63°$ S and $119.76°$ E. The wave

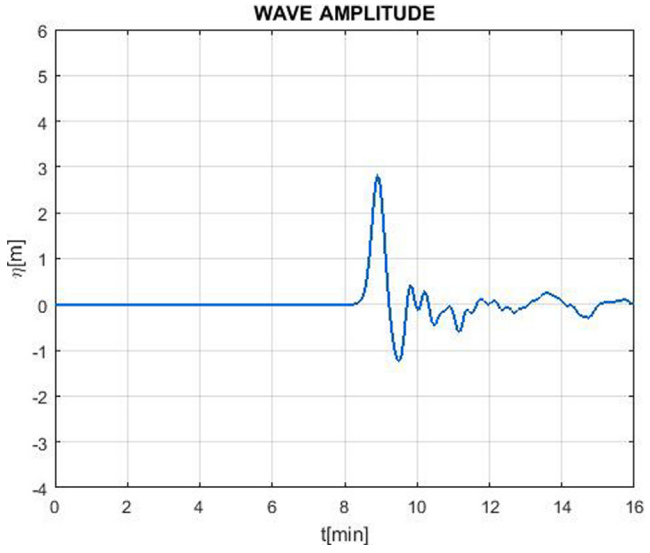

Fig. 10 Wave Amplitude caused by the triangular box landslide on Palu topography observed near the southern part of Palu Bay.

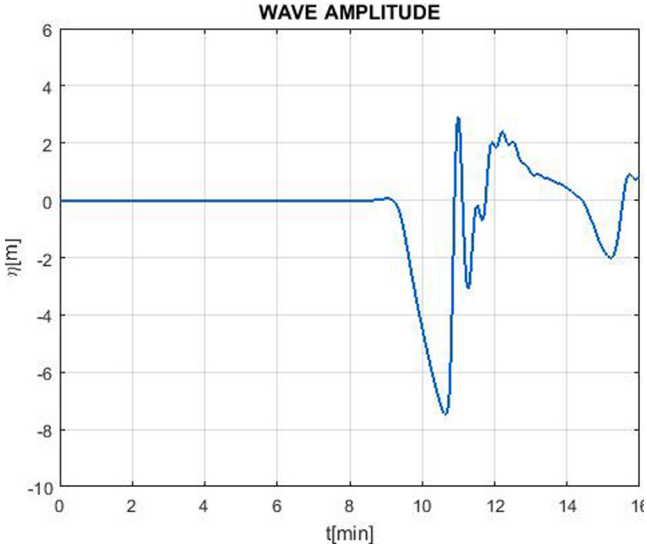

Fig. 11 Wave Amplitude of the sliding mound landslide on Palu topography observed near the southern part of Palu Bay.

surface elevation results are presented in Fig. 11. It is shown that, unlike the first case, the waves do not significantly decrease in height after reaching the maximum amplitude. Instead, the wave heights fluctuate more compared to the first case.

However, from Fig. 11, we also notice that along the time of observation, the maximum amplitude is around 2.7 meters, similar to that in the triangular box case, but the wave takes two seconds longer to reach that height. This value is also confirmed by the post-event field survey (Widiyanto, W. et al. 2019), which indicates that although the wave form is slightly different, our model and numerical scheme can properly estimate the maximum height of the tsunami waves generated by landslides under both assumptions.

6. Conclusion

In this paper, the non-linear shallow water equations were able to simulate the propagation of tsunami waves induced by submarine landslides. The analytical solution of waves generated by seafloor movement has been derived using Fourier and Laplace transforms. The finite volume method on a staggered grid has been applied to solve the model numerically. Four test cases have been performed to verify the capability and accuracy of our numerical scheme. In the first test case, we show that our numerical scheme is able to simulate wave propagation over a dry bed accurately. Further, simulation of waves generated by seafloor movement closely resembled the values obtained using the analytical solution. The computational scheme has also been tested against experimental data and other underwater landslide-simulating numerical models in two different scenarios, the triangular box and the sliding mound. The comparisons give very good agreement for both cases. The validated numerical scheme is then implemented to simulate the tsunami wave produced by landslides over the actual topography of Palu Bay. Both the triangular box and sliding mound scenarios were simulated. In both situations, the simulations provide precise estimations of the maximum tsunami wave amplitude of 2.7meters, as confirmed by the post-event field survey of 2018 Palu tsunami. This implies that the computational scheme developed in this study has successfully approximated the propagation of tsunami waves as well as their maximum amplitude. Using the results of this study, we can forecast the heights of similarly produced tsunami waves in order to aid in the development of suitable protective structures or regulations, therefore minimizing the damage caused by the waves. For further research, the vertical component can be considered, namely by involving hydrodynamic pressure.

Declaration of Competing Interest

The authors declare that they have no known competing financial interests or personal relationships that could have appeared to influence the work reported in this paper.

References

[1] US Geological Survey, M 7.5 - 70km N of Palu, Indonesia, 2018. URL https://earthquake.usgs.gov/earthquakes/eventpage/us1000h3p4/executive (accessed: 11.09.2020).

[2] Japan Meteorogical Agency, CMT solutions, 2018. URL https://www.data.jma.go.jp/svd/eqev/data/mech/world_cmt/fig/cmt20180928100243.html (accessed: 11.09.2020).

[3] H. Bao, J.P. Ampuero, L. Meng, E.J. Fielding, C. Liang, C. Milliner, T. Feng, H. Huang, Early and persistent supershear rupture of the 2018 mw 7.5 palu earthquake, Nat. Geosci. 12 (2019) 200–205.

[4] H. Takagi, M. Pratama, S. Kurobe, M. Esteban, R. Aranguiz, K. Bowei, Analysis of generation and arrival time of landslide tsunami to palu city due to the 2018 sulawesi earthquake, Landslides (2019), https://doi.org/10.1007/s10346-019-01166-y.

[5] S. Sassa, T. Takagawa, Liquefied gravity flow-induced tsunami: first evidence and comparison from the 2018 indonesia sulawesi earthquake and tsunami disasters, Landslides 16 (2018), https://doi.org/10.1007/s10346-018-1114-x.

[6] T. Arikawa, A. Muhari, Y. Okumura, Y. Dohi, B. Afriyanto, K. Sujatmiko, F. Imamura, Coastal subsidence induced several tsunamis during the 2018 sulawesi earthquake, J. Disaster Res. 13 (2018) sc20181204, https://doi.org/10.20965/jdr.2018.sc20181204.

[7] K. Pakoksung, A. Suppasri, F. Imamura, Simulation of the submarine landslide tsunami on 28 september 2018 in palu bay, sulawesi island, indonesia, using a two-layer model, Pure Appl. Geophys. 176 (2019) 3323–3350. https://doi.org/10.1007/s00024-019-02235-y.

[8] P. Heinrich, Nonlinear water waves generated by submarine and aerial landslides, J. Waterway Port Coastal Ocean Eng. (1992), https://doi.org/10.1061/(ASCE)0733-950X(1992)118:3(249).

[9] M.F. Gobbi, J.T. Kirby, Wave evolution over submerged sills: tests of a higher-order boussinesq model, Coast. Eng. 37 (1999) 57–96.

[10] D. Fuhrman, P. Madsen, Tsunami generation, propagation, and run-up with a high-order boussinesq model, Coast. Eng. 56 (2009) 747–758, https://doi.org/10.1016/j.coastaleng.2009.02.004.

[11] J.-M. Hervouet, J. Jankowski, Comparing numerical simulations of free surface flows using non-hydrostatic navier-stokes and boussinesq equations, in: Proceedings of the 4th Conference on Hydroinformatics, Iowa City, Iowa (USA), 2000.

[12] A.S. Kozelkov, A.A. Kurkin, V.V. Kurulin, S.V. Lashkin, N.V. Tarasova, E.S. Tyatyushkina, Numerical modeling of the free rise of an air bubble, Fluid Dyn. 51 (2016) 709–721, https://doi.org/10.1134/S0015462816060016.

[13] P. Lynett, P. Liu, A numerical study of submarine-landslide-generated waves and run-up, Roy. Soc. Lond. Proc. Ser. A (2002), https://doi.org/10.1098/rspa.2002.0973.

[14] M. Uddin, M. Hafez, Z. Hammouch, D. Baleanu, Periodic and rogue waves for heisenberg models of ferromagnetic spin chains with fractional beta derivative evolution and obliqueness, Waves Random Complex Media (2020) 1–15, https://doi.org/10.1080/17455030.2020.1722331.

[15] M. Hafez, S.A. Iqbal, Asaduzzaman, Z. Hammouch, Dynamical behaviors and oblique resonant nonlinear waves with dual-power law nonlinearity and fractional temporal evolution, Discrete and Continuous Dyn. Syst. Ser. S 24 (2021) 2245–2260. https://doi.org/10.3934/dcdss.2021058.

[16] M. Khader, K. Saad, Z. Hammouch, D. Baleanu, A spectral collocation method for solving fractional kdv and kdv-burger's equations with non-singular kernel derivatives, Appl. Numer. Math. 161 (2020), https://doi.org/10.1016/j.apnum.2020.10.024.

[17] M. Yavuz, N. Sene, Approximate solutions of the model describing fluid flow using generalized?-laplace transform method and heat balance integral method, Axioms 9 (2020), https://doi.org/10.3390/axioms9040123, https://www.mdpi.com/2075-1680/9/4/123.

[18] Z. Hammouch, M. Yavuz, N. Ozdemir, Numerical solutions and synchronization of a variable-order fractional chaotic system, Math. Model. Numer. Simul. Appl. 1 (2021) 11–23, https://doi.org/10.53391/mmnsa.2021.01.002.

[19] A. Ullah, Z. Ullah, T. Abdeljawad, Z. Hammouch, K. Shah, A hybrid method for solving fuzzy volterra integral equations of separable type kernels, J. King Saud Univ. Sci. 33 (2020), https://doi.org/10.1016/j.jksus.2020.101246.
[20] P. Veeresha, A numerical approach to the coupled atmospheric ocean model using a fractional operator, Math. Model. Numer. Simul. Appl. (MMNSA) 1 (1) (2021) 1–10, https://doi.org/10.53391/mmnsa.2021.01.001.
[21] L. Laiq, R. Nawaz, K. Nisar, M. Tahir, M. Yavuz, M. Kaabar, F. González, New approximate-analytical solutions to partial differential equations via auxiliary function method, J. Partial Differ. Eqs. 4 (2021), https://doi.org/10.1016/j.padiff.2021.100045.
[22] M. Yavuz, N. Sene, Fundamental calculus of the fractional derivative defined with rabotnov exponential kernel and application to nonlinear dispersive wave model, J. Ocean Eng. Sci. 6 (2020), https://doi.org/10.1016/j.joes.2020.10.004.
[23] G. Andadari, I. Magdalena, Analytical and numerical studies of resonant wave run-up on a plane structure, J. Phys. Conf. Ser. 1321 (2019) 022079, https://doi.org/10.1088/1742-6596/1321/2/022079.
[24] I. Magdalena, H.Q. Rif'atin, D.E. Reeve, Seiches and harbour oscillations in a porous semi-closed basin, Appl. Math. Comput. 369 (2020) 124835, https://doi.org/10.1016/j.amc.2019.124835.
[25] I. Magdalena Iryanto, D.E. Reeve, Free surface long wave propagation over linear and parabolic transition shelves, Water Sci. Eng. 11 (2019) 318–327, https://doi.org/10.1016/j.wse.2019.01.001.
[26] I. Magdalena, H.Q. Rif'atin, Analytical and numerical studies for harbor oscillation in a semi-closed basin of various geometric shapes with porous media, Math. Comput. Simulat. 170 (2020) 351–365, https://doi.org/10.1016/j.matcom.2019.10.020.
[27] S. Pudjaprasetya, I. Magdalena, Momentum conservative schemes for shallow water flows, East Asian J. Appl. Math. (2014) 152–165, https://doi.org/10.4208/eajam.290913.170314a.
[28] I. Magdalena, Non-hydrostatic model for solitary waves passing through a porous structure, J. Disaster Res. 11 (2016) 957–963, https://doi.org/10.20965/jdr.2016.p0957.
[29] I. Magdalena, N. Erwina, S. Pudjaprasetya, Staggered momentum conservative scheme for radial dam break simulation, J. Sci. Comput. 65 (2015) 867–874, https://doi.org/10.1007/s10915-015-9987-5.
[30] D. Avci, M. Yavuz, N. Ozdemir, Fundamental Solutions to the Cauchy and Dirichlet Problems for a Heat Conduction Equation Equipped with the Caputo-Fabrizio, Differentiation (2019) 95–107.
[31] A.Y.S.A.G. Kulikovskii, N.V. Pogorelov, Mathematical Aspects of Numerical Solution of Hyperbolic Systems, Chapman and Hall/CRC., 2001, https://doi.org/10.1201/9781482273991.
[32] K.O., Finite Volume Method, in: Computational Methods in Environmental Fluid Mechanics, Springer, 2002. https://doi.org/10.1007/978-3-662-04761-3_8.
[33] Y. Sheng, T. Zhang, Z.-Z. Jiang, A stabilized finite volume method for the stationary navier–stokes equations, Chaos Solitons Fract. 89 (2016) 363–372. https://www.sciencedirect.com/science/article/pii/S0960077916000047. https://doi.org/10.1016/j.chaos.2016.01.002, nonlinear Dynamics and Complexity.
[34] J. Tan, An upwind finite volume method for convection-diffusion equations on rectangular mesh, Chaos Solitons Fract. 118 (2019) 159–165, https://doi.org/10.1016/j.chaos.2018.09.011, https://www.sciencedirect.com/science/article/pii/S0960077918309172.
[35] S. Pudjaprasetya, I. Magdalena, Momentum conservative schemes for shallow water flows, East Asian, J. Appl. Math. 4 (2014) 152–165, https://doi.org/10.4208/eajam.290913.170314a.
[36] C.E. Synolakis, The runup of solitary waves, J. Fluid Mech. 185 (1987) 523–545, https://doi.org/10.1017/S002211208700329X.
[37] H.-Y. Lo, P. Liu, On the analytical solutions for water waves generated by a prescribed landslide, J. Fluid Mech. 821 (2017) 85–116, https://doi.org/10.1017/jfm.2017.251.
[38] A. Kurganov, G. Petrova, A central-upwind scheme for nonlinear water waves generated by submarine landslides (2008) 635–642, https://doi.org/10.1007/978-3-540-75712-2-63.